Journal of the European Ceramic Society 36 (2016) 515–525

Contents lists available at www.sciencedirect.com

Journal of the European Ceramic Society

journal homepage: www.elsevier.com/locate/jeurceramsoc

Electric field forced *c*-axis oriented growth of polar nanoregions and rapid switching of tetragonal domains in BNT-PT-PMN ternary system

Ruzhong Zuo*, Feng Li, Jian Fu, Donggeng Zheng, Wanli Zhao, He Qi

Institute of Electro Ceramics & Devices, School of Materials Science and Engineering, Hefei University of Technology, Hefei 230009, PR China

ARTICLE INFO

Article history:
Received 20 July 2015
Received in revised form 12 October 2015
Accepted 14 October 2015
Available online 27 October 2015

Keywords:
Relaxor ferroelectric
Ergodic and nonergodic phase
Strains
Domain switching

ABSTRACT

A normal to relaxor ferroelectric phase transition was observed to accompany a tetragonal to pseudocubic phase transformation in $(1-x)(0.84(Bi_{0.5}Na_{0.5})TiO_3\text{-}0.16PbTiO_3)\text{-}xPb(Mg_{1/3}Nb_{2/3})O_3$ (BNT-PT-*x*PMN) ceramics. The addition of PMN was found to gradually refine the domain morphology, such that the morphotropic phase boundary intrinsically evolved into coexisting tetragonal ferroelectric microdomains and pseudocubic nonergodic polar nanoregions (PNRs). The mechanism of generating remarkably enhanced electrostrains was ascribed to the oriented growth of PNRs and subsequently rapid switching of tetragonal domains along the electric field direction by means of in situ synchrotron X-ray diffraction, through which the symmetry of PNRs was found to be intrinsically tetragonal. The key reason for an additional polarization current peak was attributed to a significant reduction of the unit cell anisotropy at a critical field at which a simultaneous shrinkage of the lattice constant c_t led to a relatively low electrostrain compared to those previously reported in other bismuth-containing relaxor ferroelectrics.

© 2015 Elsevier Ltd. All rights reserved.

1. Introduction

Giant electrostrains of up to ~0.4% have attracted lots of attention in recent years in some perovskite-structured relaxor ferroelectric ceramics such as $(Bi_{1/2}Na_{1/2})TiO_3$ (BNT) and $Bi(Mg_{0.5}Ti_{0.5})O_3$ (BMT) based solid solutions [1–7]. The compositional modification could induce an evolution of dielectric relaxation behavior, during which a normal ferroelectric to relaxor phase transition temperature (T_{fr}) or an ergodicity to nonergodicity freezing temperature (T_f) was gradually shifted close to room temperature (RT). Because of the appearance of ergodic relaxor phases, the response of ferroelectric ceramics to external electric fields was gradually dominated by a reversible transition process from ergodic to long-range ferroelectric ordering, leading to a significant enhancement of electrostrains [2,6,8]. According to the literature survey, contributions to large strains seemed to be concerned with the electric field induced phase transition, domain switching, electrostrictive effects and converse piezoelectric effects. However, the features of strains in response to electric fields are extremely different with varying compositions, even in the same matrix compositions but modified by different additives, involving the response speed of strains to electric fields, the hysteresis degree of strains during loading and unloading [9,10], the threshold fields for generating large strains and the thermal stability of strains in addition to the strain magnitude [10,11]. Although large-strain-generating compositions were frequently reported, yet these issues seemed to need more cares. Particularly, how to optimize each contribution to strains would be a more urgent and fundamental issue. Further investigation of the physical mechanism for generating large strains would be of much interest as well because a couple of questions are still not well understood.

BNT and $Pb(Mg_{1/3}Nb_{2/3})O_3$ (PMN) are typical relaxor ferroelectrics in lead-free and lead-containing perovskite family, respectively. Both of them can form a complete solid solution with $PbTiO_3$ (PT) and simultaneously exhibit an obvious change in structural symmetry, dielectric ferroelectric and electromechanical strain behaviors. As shown in Fig. 1, a morphotropic phase boundary (MPB) between rhombohedral (*R*) and tetragonal (*T*) phases was observed as 10–15 mol% PT was added into BNT [12] or as ~32 mol% PT substituted for PMN [13]. According to the phase diagram of BNT-PT systems [12], a typical ferroelectric to antiferroelectric phase (called as nonpolar phases later) transition anomaly disappeared as PT content exceeded 15 mol%. The temperature at this dielectric anomaly was usually called as the depolarization temperature (T_d) of BNT-based piezoelectric ceramics. It intrinsically corresponded to T_{fr} at which an electric field induced ferroelectric to relaxor phase transition occurred, and mostly tended to decrease as donor dopants or other perovskite phases were added [1,7,14].

* Corresponding author. Fax: +86 551 62905285.
E-mail addresses: piezolab@hfut.edu.cn, rzzuo@hotmail.com (R. Zuo).

http://dx.doi.org/10.1016/j.jeurceramsoc.2015.10.013
0955-2219/© 2015 Elsevier Ltd. All rights reserved.

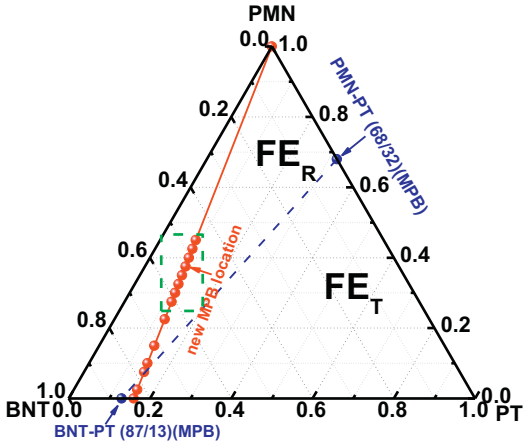

Fig. 1. Schematic phase diagram of BNT-PT-PMN ternary system.

However, giant strains reported in BNT-based binary or ternary systems were generally not observed in the proximity of T_{fr} but close to the T_f although this issue was mostly vague in the literatures. As reported, there was a much smaller difference between T_f and T_{fr} for BNT-based relaxor ferroelectrics than for BMT-based systems. This kind of difference was believed to probably contribute to different thermal stability of large strains [10]. Moreover, the achievement of large electrostrains usually requires a relatively high driving electric field of up to 6–7 kV/mm in most of BNT based solid solutions probably because of their specific domain structures [5–7,9,15,16]. By comparison, most of R PMN-PT solid solutions have a low coercive field (E_c) and exhibit a typical dielectric relaxor behavior. As a result, the substitution of PMN for BNT can be expected to modify the domain morphology and further to optimize the dielectric and electromechanical strain behavior.

In this work, a specially-designed new composition system of $(1-x)$(0.84BNT-0.16PT)-xPMN (abbreviated as BNT-PT-xPMN) was constructed by mixing two systems PMN and BNT-PT together in terms of their respective phase transition behavior and possibly different domain structures. The aim to do so is to see how the phase or domain structures of this system vary with changing the PMN content and the electric field magnitude, and how the ergodic phases or nonergodic phases respond to the variation of external electric fields, and particularly to further make clear the mechanism of generating large strains by means of temperature or composition dependent synchrotron X-ray diffraction (XRD), dielectric properties and polarization (strain) versus electric field (P(S)–E) curves.

2. Experimental

The BNT-PT-xPMN (x = 0–0.45) composition points were drawn as red dots in Fig. 1, being distributed on both sides of a theoretically predicted MPB line of BNT-PT and PMN-PT binary systems by fixing a constant ratio of BNT to PT. The ceramics with different x were synthesized by a conventional solid-state reaction method using high-purity oxides: Bi_2O_3 (99.0%), Na_2CO_3 (99.8%), PbO (99.0%), $(MgCO_3)\,4{\cdot}Mg(OH)\,2{\cdot}5H2O$ (99.0%), Nb_2O_5 (99.5%) and TiO_2 (99.0%) as raw materials. The powders were weighed and ball-milled with ethanol and zirconia media for 4 h, and calcined twice after drying in a closed alumina crucible at 850 °C for 2 h. After calcination, the powder mixture was ball-milled again for 6 h with 0.5 wt% PVB as a binder. The granulated powder was uniaxially pressed into discs with a diameter of 10 mm and a thickness of 1 mm. The compacted discs were sintered in the temperature range of 1100–1200 °C for 2 h. To minimize the vaporization of Pb, Na and Bi, sample discs were buried in the sacrificial powder of the same composition. For the electrical measurements, silver paste was painted on major sides of the discs and fired at 550 °C for 30 min as electrodes. The specimens were polarized in a silicone oil bath at RT under a dc field of 3–4 kV/mm for 15 min.

The relative densities of sintered samples were evaluated by the Archimedes method. The phase structures were analyzed at RT using a conventional powder X-ray diffractometer (XRD, D/Mzx-rB; Rigaku, Tokyo, Japan) with CuKα1 radiation. The grain morphology was observed by using a field-emission scanning electron microscope (FE-SEM, SU8020, JEOL, Tokyo, Japan). Before the SEM observation, the samples were polished and thermally etched at ~950 °C for 30 min. The dielectric properties were measured using an LCR meter (Agilent E4980A, Santa Clara, CA) in a temperature range of 20–400 °C and at a frequency range of 0.1 kHz-1 MHz. The quasi-static piezoelectric strain constant d_{33} of poled samples was measured by a Berlincourt-meter (YE2703A, sinocera, Yangzhou, China). The planar electromechanical coupling factor k_p was determined by a resonance-antiresonance method with an impedance analyzer (PV70A; Beijing Band ERA Co. Ltd., Beijing, China). A ferroelectric testing system (Precision multiferroelectric, Radiant Technologies Inc., Albuquerque, NM) was used to measure the polarization-electric field (P–E) hysteresis loops and electric field-induced strain (S–E) curves. *In-situ* high-resolution synchrotron XRD measurement was carried out under various electric fields or at different temperatures at Shanghai Synchrotron Radiation Facility (SSRF) using beam line 14B1 (λ = 1.2378 Å).

3. Results

3.1. Phase structural transition, microstructure and normal ferroelectric to relaxor phase transition

Fig. 2 demonstrates RT XRD patterns of BNT-PT-xPMN ceramics. A single perovskite structure could be clearly identified for all compositions according to their typical diffraction patterns. Moreover, a typical T symmetry could be identified as $x < 0.325$, as evidenced by both the peak splitting of the (0 0 2) and (2 0 0) diffraction lines and the single (1 1 1) diffraction peak. When $x \geq 0.4$, a sharp and narrow peak profile of both (2 0 0) and (1 1 1) diffraction lines suggested a pseudocubic (PC) structure. Slowly scanned (2 0 0) diffraction lines in a 2θ range of 45–46.5° were fitted by using a Gaussian peak shape function for samples with x = 0.275–0.425, as shown in Fig. 2(c1)–(c8). The structural symmetry of the samples can be well established from the peak splitting and the relative intensity of these reflection lines. The $(0\,0\,2)_T/(2\,0\,0)_T$ and $(2\,0\,0)_{PC}$ peaks could be simultaneously detected in the x = 0.325–0.385 samples, indicating that there existed an MPB between T and PC phases.

The microstructure of the selected samples is shown in Fig. 3. It is evident that the introduction of PMN had an obvious influence on the evolution of the microstructure. Pure BNT-PT (x = 0) showed relatively large grains and a relatively low density (~95%). With the introduction of PMN, the grain size decreased and the sample density slightly increased (>97% as $x \geq 0.3$). The average grain size, as estimated with a linear interception method, increased from ~6 μm for the x = 0 sample to ~3–4 μm for the x = 0.3, x = 0.375 and x = 0.425 samples. It is worthy of note that the grain morphology significantly changed from polyhedra to irregular shapes with adding PMN into BNT-PT. Two kinds of grains with different contrasts were observed in samples with $x > 0$ probably as a result of different crystalline surfaces they have. There were no traces of secondary phases as identified by the XRD results in Fig. 2.

Fig. 4(a)–(g) shows the temperature and frequency dependence of dielectric permittivity (ϵ_r) of BNT-PT-xPMN ceramics before and after poling. It can be seen that a spontaneous relaxor to ferroelectric transformation occurred at temperatures T_{fr} in virgin samples with $x \leq 0.3$ in terms of clearly observed frequency-independent

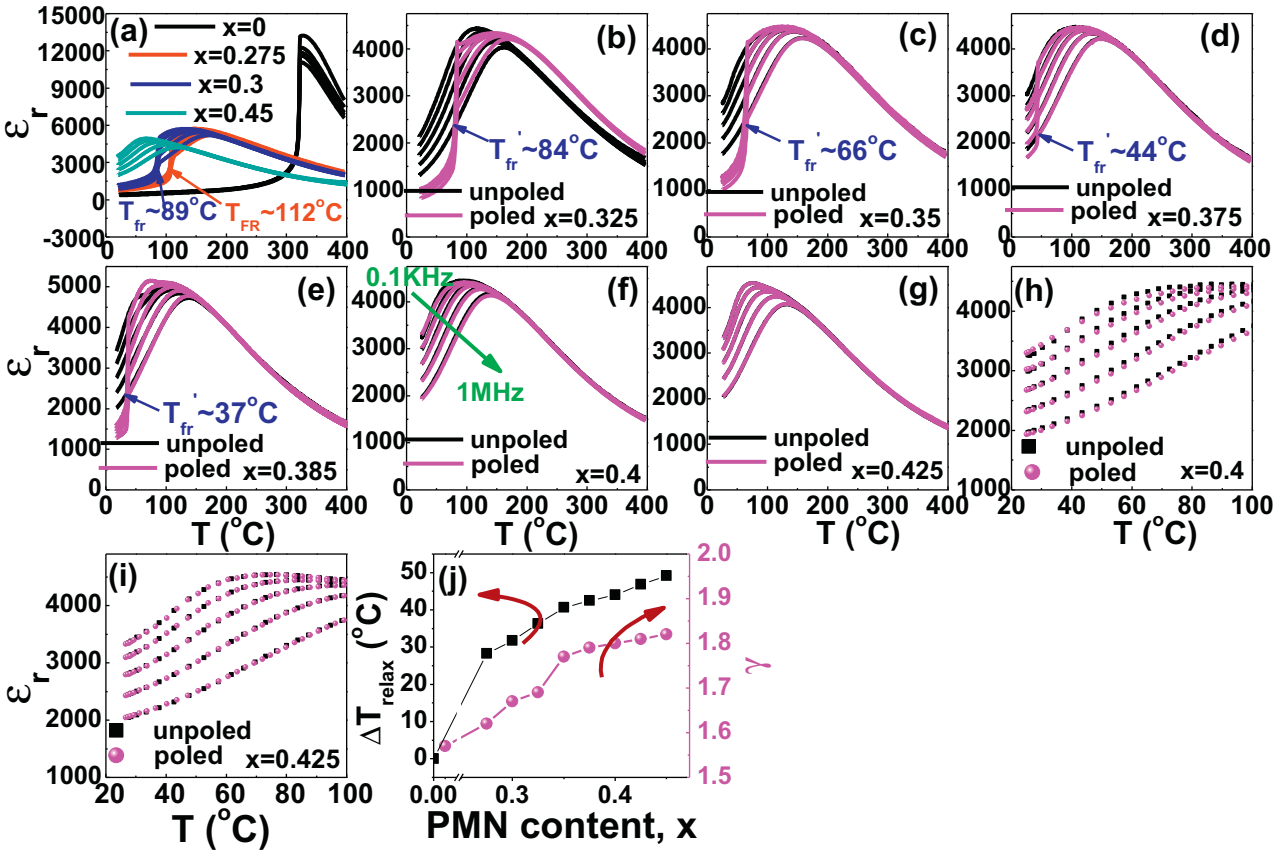

Fig. 4. (a)–(g) Dielectric permittivity of unpoled and poled BNT-PT-*x*PMN ceramics as indicated as a function of temperature and frequency; (h) and (i) the locally magnified dielectric permittivity versus temperature curves in the temperature range of 20 °C in Fig. 4(f) and (g), respectively; (j) the variation of both γ and ΔT_m as a function of the PMN content.

into a nonergodic phase transition at T_f upon cooling [17–19]. Particularly, there is not any detectable difference in the dielectric permittivity-temperature curves for the $x \geq 0.4$ samples before and after poling, meaning that these samples should be dominantly composed of ergodic phases at RT [17,20], as shown in Fig. 4(f–i). For $x = 0.325$–0.385 samples, they were located at the coexistence zone of *T* and PC phases and simultaneously exhibited typical dielectric relaxor behavior as manifested by Fig. 4(b–e). It can be seen that the dielectric relaxor behavior around T_m of this ternary system became stronger and stronger with the substitution of PMN, as characterized by the diffuseness degree γ, which is calculated by a modified Curie–Weiss law ($1/\epsilon - 1/\epsilon_m = C^{-1}(T-T_m)^{\gamma}$) [21] and another parameter ΔT_{relax}, which can be defined as the difference between two T_m values measured at 1 kHz and 1 MHz. As shown in Fig. 4(j), both values steadily increased with increasing the PMN content. This is because the disordered distribution of different ions with various sizes and valences at one or more equivalent crystallographic sites would cause the formation of random local (strain or electric) fields, which are responsible for either breaking long-range ferroelectric domains into PNRs or further promoting the growth of PNRs [22,23]. The substitution of PMN tended to enhance the random local fields of the ternary system, resulting in a gradual increase of the dynamics of PNRs and a decrease in size of PNRs. Therefore, a *T* to PC structural transformation at RT was just accompanied by a normal ferroelectric to relaxor phase transition for the BNT-PT-*x*PMN ternary system. As a result, the MPB within $0.325 \leq x \leq 0.385$ actually evolved into a coexistence of *T* ferroelectric microdomains and PC nonergodic PNRs. Concerning the $x = 0.385$ sample, a small part of nonergodic phases might have changed into ergodic phases at RT with the decrease of T_f values, as pointed out infra.

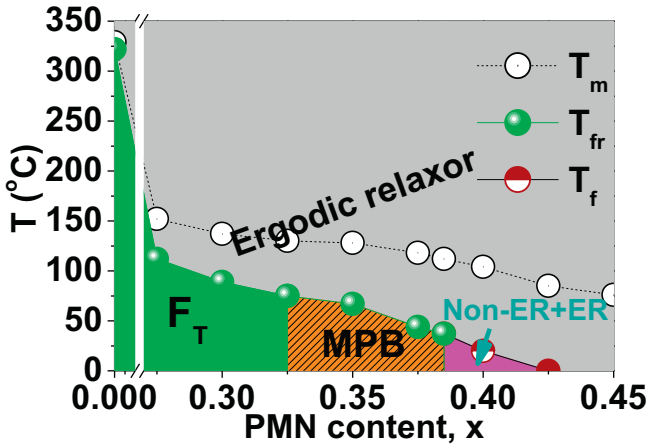

Fig. 5. The phase diagram of BNT-PT-*x*PMN ceramics (T_m was determined at 1 kHz).

Because a full relaxor state is expected at RT as $x \geq 0.385$, the T_f value can be obtained by fitting the measured dielectric permittivity versus temperature curves at different frequencies to the Vogel-Fulcher relationship [17,19]. It can be also roughly estimated by a field-induced ferroelectric to relaxor phase transition temperature T_{fr}', which was grasped in dielectric permittivity versus temperature curves for poled samples (see Fig. 4(b)–(e)). In combination with the analysis of XRD results (Fig. 2), a composition-temperature-phase diagram could be approximately drawn, as plotted in Fig. 5. It can be seen that the BNT-PT-*x*PMN compositions at RT exhibited a T phase with ferroelectric

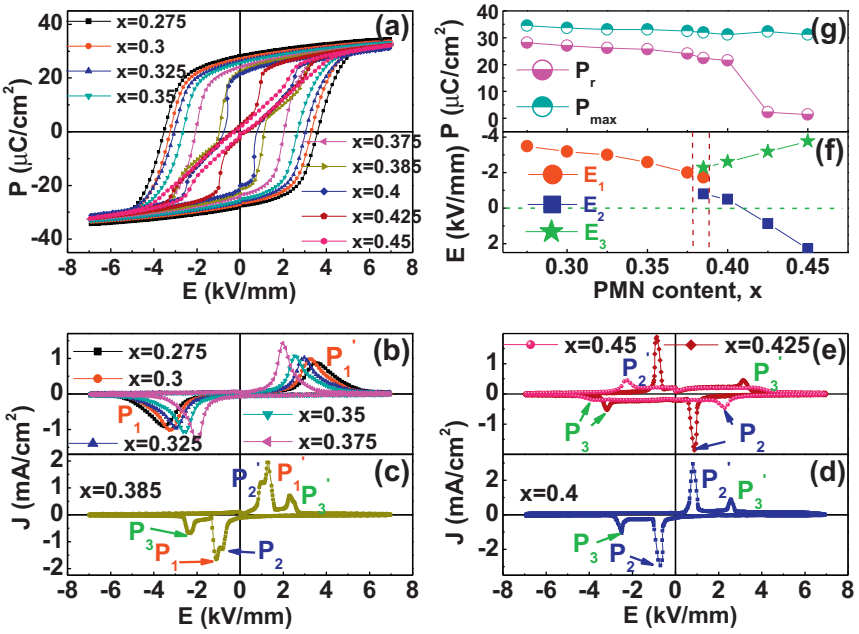

Fig. 6. (a) P–E hysteresis loops at 1 Hz of BNT-PT-*x*PMN ceramics as indicated, (b)–(e) J–E loops for the corresponding ceramics samples in which *P*–P_3 stand for the polarization current peaks, (*f*) the electric field values E_1–E_3 at *P*–P_3 peaks in Fig. 6(b–e) changing with *x*, and (g) the variation of both maximum polarization P_{max} and remanent polarization P_r as a function of *x*.

macrodomains as $0 \leq x < 0.325$, then a two-phase coexistence of T phases with microdomains and PC phases of nonergodic PNRs as $0.325 \leq x < 0.385$, and finally transformed into a single PC phase composed of nonergodic and/or ergodic PNRs. These results demonstrate that the addition of PMN played a significant role in refining the domain morphology of BNT-PT-*x*PMN ternary system.

3.2. Polarization switching behavior of BNT-PT-xPMN ternary system

Fig. 6(a–e) depicts RT P–E loops for samples with $x = 0.275 \sim 0.45$ and the corresponding current density loops (J–E). Obviously, a nearly saturated and square P–E loop together with a single sharp polarization current peak (P_1) were observed during loading electric fields for the $x = 0.275$–0.375 samples, which are characteristic of normal ferroelectrics ($x = 0$–0.3) or nonergodic relaxors ($x = 0.325$–0.375). Although the $x = 0.385$ sample was also located at the *T* and PC phase coexistence zone (MPB), its P–E loop was obviously pinched and its J–E curves exhibited three polarization current peaks (P_1–P_3 as indicated in Fig. 6(c)). This should be extremely interesting for most of relaxor ferroelectrics since it was rarely reported previously. Two split current peaks have been frequently observed in a couple of relaxor ferroelectrics [6,10,11,24,25] as their T_f values were adjusted close to RT, which correspond to the back-switching process of both field induced ergodic-to-ferroelectric (P_2) and nonergodic-to-ferroelectric (P_1) phase transition, respectively [6,26,27]. As $x \geq 0.4$, P–E loops of these samples were still pinched firstly ($x = 0.4$–0.425) and then became extremely slim ($x \geq 0.45$), accompanied by two obviously separated current peaks (P_2 and P_3) even for samples entering into a pure ergodic phase zone ($x \geq 0.425$) at RT. This significantly differs from the common sense that only a single polarization current peak formed during unloading could be observed for a pure ergodic phase or an ergodic phase dominated composition, together with a polarization current platform instead of a sharp current peak during loading [6,10,11,28]. That is to say, the polarization current peak P_3 indicated in Fig. 6(c–e) for the $x = 0.385$–0.45 samples should not be attributed to the field induced ergodic to ferroelectric phase transition.

The variation of the electric field values E_1–E_3 corresponding to the current peaks P_1–P_3, respectively, as a function of *x* is shown in Fig. 6(f). The E_1 value started to decrease slowly with increasing *x* owing to the decrease of tetragonality ($x = 0$–0.32) and domain sizes (PNRs, $x = 0.325$–0.385). The appearance of E_2 indicated the existence of ergodic phases. It can be seen that the coexistence of ergodic and nonergodic phases occurred within a very narrow composition range. Among these studied compositions, it was detected only in the $x = 0.385$ sample, however, from which E_3 started to appear and became larger with increasing *x*. How to make clear the origin of the P_3 peak (E_3) will be of much importance. Moreover, the maximum polarization P_{max} and remanent polarization P_r were plotted as a function of the PMN content, as shown in Fig. 6(g). The P_{max} values remained almost constant in the whole composition range, suggesting that a well-oriented long-range ferroelectric ordering can be sufficiently established under 7 kV/mm even for compositions of pure ergodicity. By comparison, a gradual decrease of P_r values with increasing *x* and then a sudden drop at $x > 0.4$ demonstrate that recoverable contributions such as from the unstable domain switching or from ergodic to ferroelectric reversible phase transition became more and more important.

3.3. Remarkably enhanced electrostrains at T_f and T_{fr}

RT bipolar and unipolar strain curves under 7 kV/mm at 1 Hz are shown in Fig. 7(a and b), respectively. All these curves were obtained from the measurement of non-first cycles. It can be seen from Fig. 7(a), that the $x \leq 0.385$ samples exhibited a typical butterfly loop with a large negative strain (S_{neg}), which is typical for a normal ferroelectric or a nonergodic relaxor. When $x \geq 0.4$, the butterfly shaped strain curves drastically converted into horn-shaped ones nearly in the absence of S_{neg}, accompanied by a rapid increase in the positive strain (S_{pos}), as can be also seen in Fig. 7(b). The maximum S_{pos} value of ~0.31% was achieved in the $x = 0.425$ sample, in which the S_{neg} value just got close to zero (see Fig. 7(c)). For a certain ferroelectric composition, poling strains are usually

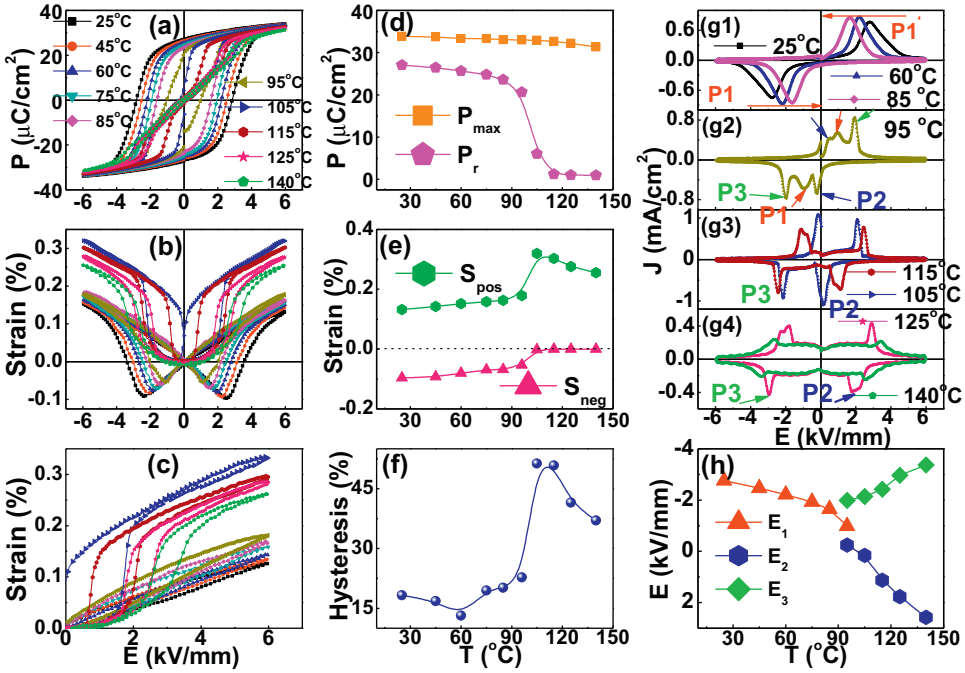

Fig. 8. (a) Bipolar P–E loops, (b) bipolar and (c) unipolar S–E curves of the $x = 0.3$ sample with changing the measuring temperature; the variation of (d) maximum polarization P_{max} and remanent polarization P_r, (e) both S_{pos} and S_{neg} and (f) the hysteresis degree of strains with increasing temperature; (g1)–(g4) the evolution of J–E curves with changing temperature in which P_1–P_3 stand for the polarization current peaks; (h) the electric field values E_1–E_3 at P–P_3 peaks in Fig. 8(g1–g4) changing with temperature.

ance of ergodic phases approximately at 95 °C. S_{neg} values gradually arrived at zero at ~105 °C and concurrently S_{pos} value reached their maxima (Fig. 8(e)). This means that ergodic phases can be also reversibly transformed into a long-range ferroelectric order driven by an external electric field near T_{fr} [28]. It suggested that ergodic phases should have similar free energies to resultant ferroelectric phases considering possible phase coexistence of ergodic and ferroelectric phases in the proximity of T_{fr}. This is very similar to the case near T_f where ergodic and nonergodic phases have similar energies. As a result, the strain hysteresis was significantly dependent on measuring temperature, and reached its maxima (~50%) approximately near 105 °C (Fig. 8(f)).

As shown in Fig. 8(g), a single polarization current peak P_1 was observed below 85 °C, indicating that a normal ferroelectric state is dominant. However, there appeared two polarization current peaks (P_2 and P_3) above 95 °C, even if the sample entered into a pure ergodic phase zone as the temperature was higher than 105 °C. Interestingly, three polarization current peaks P_1–P_3 were observed at 95 °C. This phenomenon was very similar to that observed in Fig. 6(c). The appearance of P_3 during increasing temperature suggested that there must be an additional process inducing a rapid change of polarization vectors. The electric field values E_1–E_3 corresponding to the P_1–P_3 were plotted as a function of temperature, as shown in Fig. 8(h). The decline of E_1 should be attributed to the decrease of tetragonality due to the increase of temperature. The increase of E_2 was caused by the decreased hysteresis of induced ferroelectrics back to ergodic phases owing to enhanced dynamics of ergodic PNRs. It can be also seen that E_3 increased nearly linearly with increasing temperature as well.

4. Discussion

The substitution of PMN was found to induce a phase structural change from a T normal ferroelectric to a PC relaxor ferroelectric. A morphotropic phase coexistence between T and PC phases was identified between $x = 0.325$ and $x = 0.385$ where piezoelectric properties ($d_{33} \sim 191$ pC/N, $k_p \approx 18.7\%$ at $x = 0.375$) were obviously

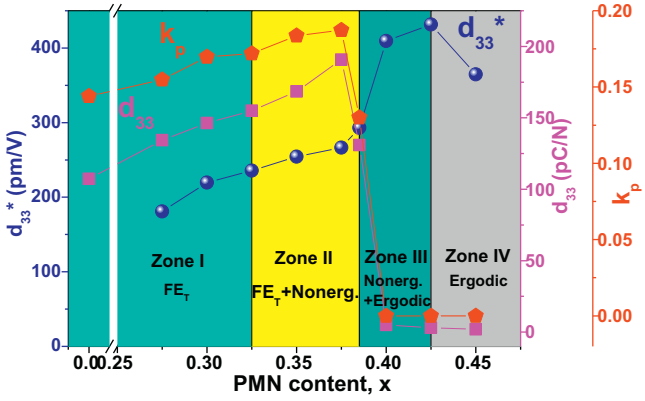

Fig. 9. (a) Quasi-static d_{33}, planar electromechanical coupling coefficient k_p and normalized strains d_{33}^* (S_{max}/E_{max}) values of BNT-PT-xPMN ceramics as a function of the PMN content.

enhanced, as shown in Fig. 9. By comparison, the maximum normalized strains d_{33}^*~440 pm/V was reached in the ergodic phase ($x = 0.425$) close to the ergodic and nonergodic phase boundary. It seemed to be slightly lower than those usually observed in a few bismuth-containing relaxor ferroelectric ceramics (usually ~0.4% at 7–8 kV/mm, d_{33}^*~500–600 pm/V) [7,9,10,30].

In situ high-resolution synchrotron XRD was carried out to ascertain how the phase structure or domain switching responded to external electric fields. As shown in Fig. 10(a), the $x = 0.375$ composition at zero field was located in the vicinity of MPB, as evidenced by the appearance of $(002)_T/(200)_T$ and $(200)_{PC}$ peaks. As a small electric field was applied, the PC phase immediately disappeared and a pure T phase was left. The intensity ratio of $(002)_T$ and $(200)_T$ only slightly increased with increasing the field up to 1 kV/mm. The interesting thing is that an obvious and rapid c-axis-oriented domain switching occurred as the applied electric field was higher than 2 kV/mm, as manifested by a significantly increased $(002)_T/(200)_T$ intensity ratio. As the electric field was

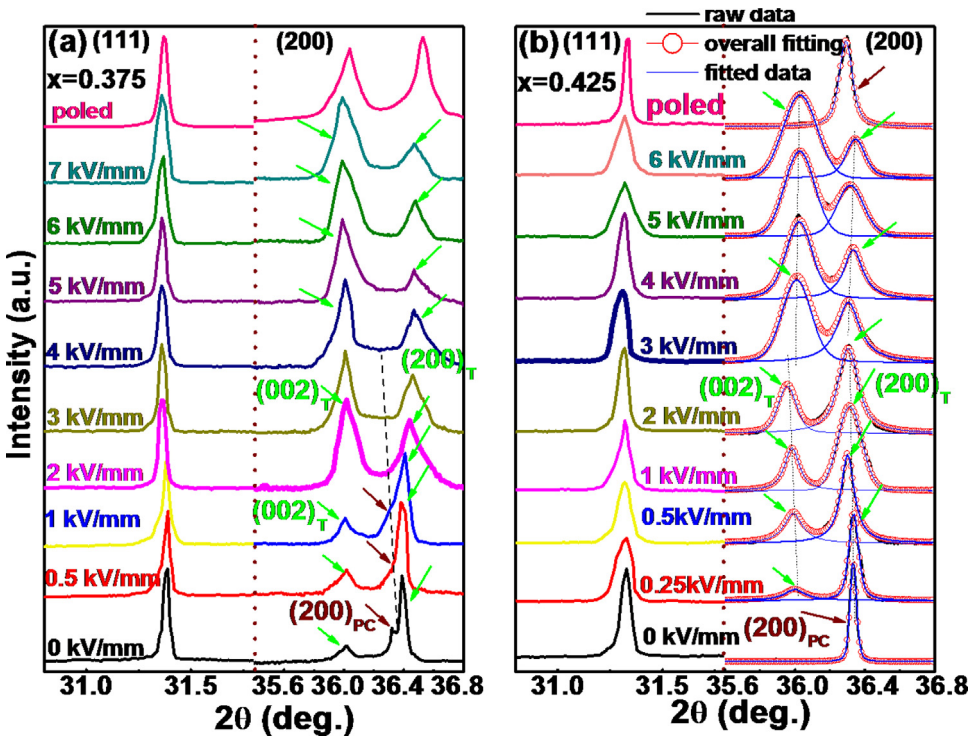

Fig. 10. Evolution of the (1 1 1) and (2 0 0) diffraction lines with increasing the electric fields for ceramic samples: (a) $x = 0.375$ and (b) $x = 0.425$ in comparison with the corresponding diffraction lines of respective samples after the maximum applied electric field was totally released (poled); the electric field dependent changes of (2 0 0) diffraction lines fitted by a pseudo-Voigt function for the $x = 0.425$ sample.

further increased, the $(0\,0\,2)_T/(2\,0\,0)_T$ ratio exhibited a relatively small increase. The field value of 2 kV/mm at which a rapid domain switching occurs just corresponded to the E_1 value of the $x = 0.375$ sample as shown in Fig. 6(b and f). As the electric field was released (after poling), it can be seen that the *c*-axis orientation of domain switching still existed but was partly recovered compared to the state under an electric field larger than 2 kV/mm. Nevertheless, the effect of domain switching in the poled $x = 0.375$ sample was still very strong compared to a usually observed ferroelectric. The two-phase coexistence (MPB) and low domain wall energy (PNRs) in the $x = 0.375$ sample would make polarization switching much easier along the electric field direction, being responsible for enhanced piezoelectric activities. Fig. 10(b) further certifies that the $x = 0.425$ sample should be an ergodic phase with a PC symmetry at zero field. Only a small field up to 0.25 kV/mm could make it transform into a *T* phase, which then exhibited a slightly increased *c*-axis-orientation with increasing the field up to 2 kV/mm. A significantly enhanced *c*-axis orientation was suddenly finished upon the application of a field of 3 kV/mm, as observed in the $x = 0.375$ sample. Although the *c*-axis orientation degree could be slightly increased with further increasing the field, yet initial PC phase was completely recovered as the electric field was released, suggesting that the field induced ergodic to ferroelectric phase transition is reversible. The electric field value of 3 kV/mm at which a fast *c*-axis orientation occurs for the $x = 0.425$ sample was just consistent with the E_3 value in Fig. 6(e and f). For a normal ferroelectric or a nonergodic relaxor ferroelectric, the E_1 value achieved from its P–E loop should be its E_c value at which the polarization vector responds to the electric field in the fastest way, as we observed in Fig. 10(a) for the $x = 0.375$ sample. As a result, the P_3 peak of the $x = 0.425$ sample in Fig. 6(e) should be ascribed to a rapid *c*-axis oriented *T* domain switching. This finding should also fit to other BNT-PT-*x*PMN samples. In $x = 0.325$–0.375 samples, the coexisting *T* ferroelectric phase and PC nonergodic phase have very similar free energies such that both of them exhibited a single switching process. Because of the appearance of a small amount of ergodic phases, three polarization current peaks were observed simultaneously in the $x = 0.385$ sample.

Fig. 11 shows the evolution of typical (1 1 1) and (2 0 0) diffraction peaks of the $x = 0.3$ sample with varying temperature and the applied electric field in order to explore the field dependence of the phase structure near T_{fr}. As can be seen from Fig. 11(a), an RT *T* phase at zero field transformed into a pure PC phase with increasing temperature up to 125 °C, undergoing a coexistence of *T* and PC phases roughly in the temperature of 70–95 °C. This result indicated that the freezing of high-temperature ergodic phases into a long-range *T* ferroelectric order is also a diffuse process, although T_{fr} was approximately identified to be 89 °C by means of the measurement of dielectric-temperature curves (Fig. 4). As a result, it will not be difficult to understand why the maximum electrostrain appeared at 105 °C instead of at 89 °C. As measuring temperature was raised to 105 °C (Fig. 11(c)), the sample became a nearly pure ergodic phase with a PC symmetry at zero field. It then underwent a similar change of (1 1 1) and (2 0 0) diffraction lines with increasing the electric field to that observed in the $x = 0.425$ sample. The appearance of a T phase from a PC phase was driven at a field as small as 0.25 kV/mm. After a slight domain switching along the field direction, a rapid and sudden *c*-axis oriented domain switching happened at 2 kV/mm which corresponds to the E_3 value observed in Fig. 8(h). It is certain that the formation of the P_3 peak in J–E curves for the $x = 0.3$ sample on the ergodic phase side should be also attributed to the rapid *c*-axis domain orientation driven by an electric field. The different thing is that as measuring temperature was raised to 125 °C, the initial ergodic phase with a PC symmetry could remain stable under a field of up to 2 kV/mm. A *T* phase simultaneously with a significant *c*-axis orientation suddenly appeared as an electric field of 3 kV/mm was applied. This field value approx-

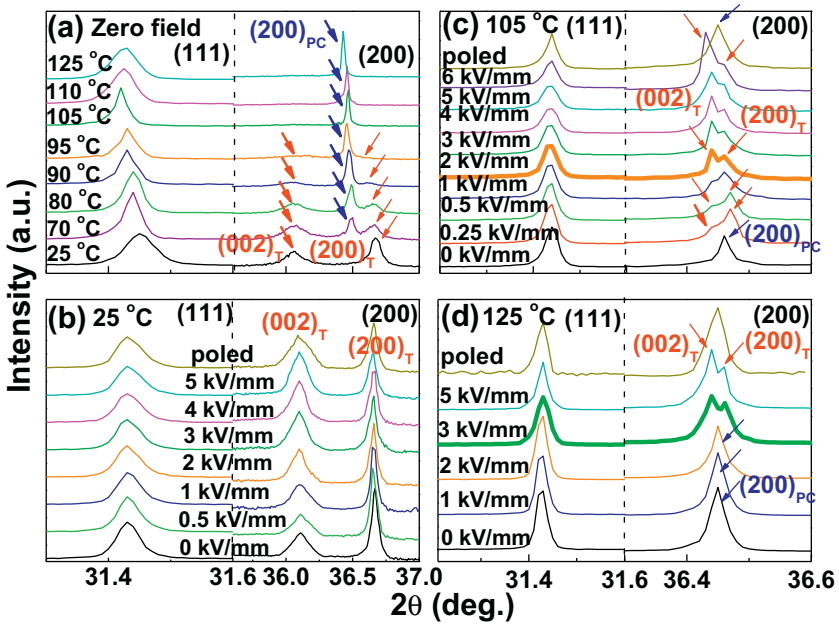

Fig. 11. Evolution of the (1 1 1) and (2 0 0) diffraction lines of the $x = 0.3$ sample: (a) at different temperatures, at zero field, and (b)–(d) at 25 °C, 105 °C and 125 °C with increasing the electric field, respectively, in comparison with the corresponding diffraction lines of respective samples after the maximum applied electric field was totally released (poled).

imated to the E_3 value at 125 °C for the $x = 0.3$ sample (Fig. 8(h)). Interestingly, if Figs. 10 (b) and 11 (c and d) were compared, it will be found that a zero-field PC phase of ergodicity evolved directly into a *T* phases under a small electric field, instead of undergoing an *R* phase firstly and then changing into a *T* phase as observed previously [10,31,32]. Moreover, it seems that this electric field value obviously depended on the dynamics of ergodic PNRs.

As known, high-temperature ergodic PNRs may have different symmetries such as *T*, *R* and so on [33,34], although their matrix compositions usually look like a PC phase [19]. Because the size of PNRs is beyond the coherence length to be detected by an XRD, the intrinsic symmetry of these PNRs can not be properly distinguished from that of the matrix. The application of external electric fields played a role in lowering the energy fluctuation of the system, such that the amount of stably existing PNRs suddenly increased as the applied electric field was above a threshold value. This process macroscopically behaves like the oriented growth of PNRs instead of a real phase transition. As a result, an inherent *T* symmetry of PNRs in this study could be visualized under the irradiation of X-ray. The higher the measuring temperature above T_{fr} is, the larger the dynamics of ergodic PNRs is and the higher the required electric field is (Fig. 11(d)). Following that, a rapid switching of *T* domains along *c*-axis occurred as the electric field was higher than the corresponding E_3 value. If the symmetry of PNRs is intrinsically *R* in some cases, a structural phase transition from *R* to *T* symmetry may be also possible after the visualization of *R* symmetry as a result of PNRs growth [6,31]. In this study, an obviously *c*-axis oriented domain switching became much easier probably because of the preferentially oriented growth of PNRs under the application of electric fields, as we observed in textured ferroelectric ceramics or domain-engineered single crystals [35,36]. This can be more clearly supported by carefully looking at Fig. 11(b) in which the $x = 0.3$ sample at 25 °C exhibited only a normal domain switching with the electric field instead of a rapid *c*-axis orientation because it belongs to a T normal ferroelectric with macro-domain structures at RT. If one compared the zero-field virgin sample with the post-poled one (see Figs. 10 (b) and 11 (c and d)), it can be found that the above-mentioned field induced PNRs growth and switching process is completely reversible in an ergodic relaxor. According to the above discussion, the physical mechanism of generating large electrostrains near both T_f ($x = 0.425$) or T_{fr} ($x = 0.3$) could be updated to an electric field induced reversible process involving both *c*-axis oriented growth of PNRs and fast switching of T domains.

The (2 0 0) diffraction peak profiles of the $x = 0.425$ sample were fitted by a pseudo-Voigt function (Fig. 10(b)). The calculated lattice parameters, cell volume, lattice strain and volume fraction (F) of domains aligned with the poling direction as a function of electric field are shown in Fig. 12. It can be seen that an obvious change of lattice parameters took place with increasing the electric field. Particularly, the c_t value first increased with the field from 0.25 kV/mm up to 2 kV/mm and then rapidly decreased at 3 kV/mm, and finally remained almost constant after 3 kV/mm. There is only a slight change of a_t compared with c_t. As a result, the unit cell volume exhibited a similar change to the c_t value, as shown in Fig. 12(b). Interestingly, a sharp decrease of the cell anisotropy (i.e., tetragonality c/a shown in Fig. 12(a)) and the cell volume occurred at 3 kV/mm. The former would largely facilitate the domain orientation along *c*-axis. However, the shrinkage of the unit cell volume tended to make the electrostrain smaller. It can be more clearly seen from Fig. 12(c) that the lattice strain along *c*-axis (the electric field direction) roughly calculated using the data of Fig. 12(a) first increased with the field up to 2 kV/mm and then became negative after 3 kV/mm. It was −0.083% as 6 kV/mm was applied, which should be the main source of a relatively low electrostrain observed in BNT-PT-*x*PMN ternary system. The volume fraction of domains parallel to the electric field direction can be calculated by $F = I_{(002)}/(I_{(002)} + I_{(200)})$, as shown in Fig. 12(d). It can be seen that poling has resulted in a fast increase in the proportion of domains aligned along the field direction (36% at 2 kV/mm to 58% at 3 kV/mm). This should be basically responsible for the appearance of the P_3 peak in Fig. 6. It is worthy of note that the unit cell volume of the zero-field sample (Fig. 12(b)) should not be a real volume of the sample because the calculated value V_{PC} only came from the lattice parameters of the matrix phases without considering the inherent symmetry of involved PNRs.

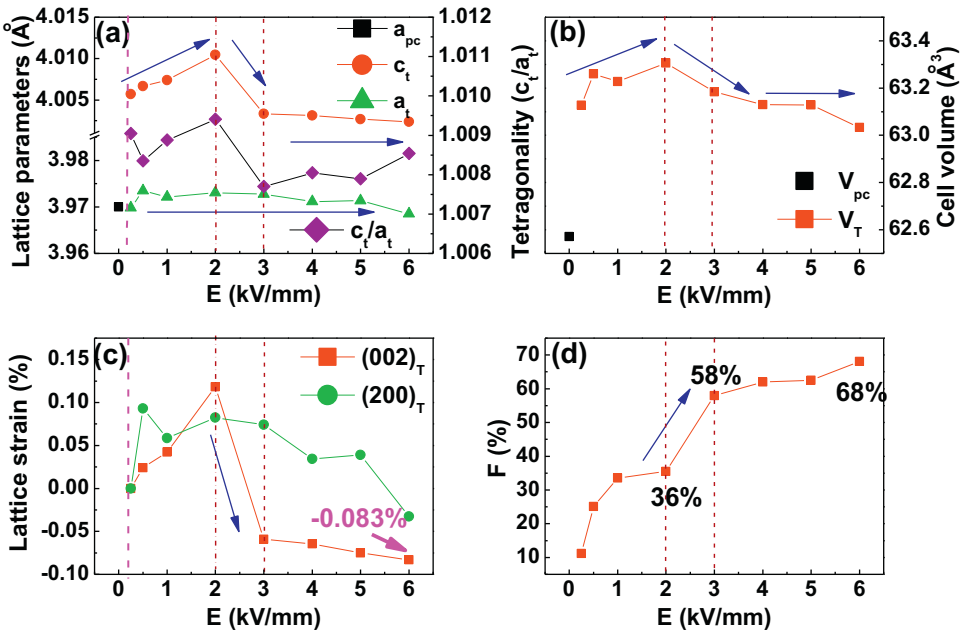

Fig. 12. The calculated (a) lattice parameters, (b) unit cell volume, (c) lattice strains and (d) volume fraction (F) of domains aligned with the poling direction as a function of the applied electric field.

5. Conclusions

A composition modulated phase structural transition from T to PC symmetry was found in BNT-PT-xPMN ternary system, accompanying a normal to relaxor ferroelectric phase transformation. A morphotropic phase coexistence between T and PC phases was identified within $0.325 \leq x \leq 0.385$ where relatively high piezoelectric activity was achieved in the $x = 0.375$ sample owing to sufficient domain switching facilitated by a lower domain wall energy. The evolution of dielectric relaxation and polarization switching behavior for unpoled and poled samples manifested the coexistence of T ferroelectric microdomains and PC nonergodic PNRs at MPB. In situ synchrotron XRD measurements suggested that the physical mechanism of generating remarkably enhanced electrostrains at T_f or T_{fr} should be more intrinsically attributed to the oriented growth of ergodic PNRs and subsequently rapid switching of T domains along the electric field direction, instead of just a reversible field induced ergodic to ferroelectric phase transition stated previously. The rapid switching of T domains especially found in BNT-PT-xPMN ternary system produced an additional polarization current peak during electric cycling. The driving force was provided by a sudden reduction of the unit cell anisotropy (tetragonality c_t/a_t) at a critical electric field at which a simultaneous shrinkage of the lattice constant c_t led to a slightly low electrostrain (~0.31% at 7 kV/mm). These experimental results provided an updated insight into the structural essence of the electric field induced ergodic to ferroelectric ordering transition responsible for the mechanism of generating giant electrostrains in relaxor ferroelectric ceramics.

Acknowledgments

Financial support from the National Natural Science Foundation of China (Grant No. 51472069, U1432113, 11205235) and the Anhui Provincial Natural Science Foundation (1508085JGD04) is gratefully acknowledged.

References

[1] R.Z. Zuo, C. Ye, X.S. Fang, J.W. Li, Tantalum doped $0.94Bi_{0.5}Na_{0.5}TiO_3$-$0.06BaTiO_3$ piezoelectric ceramics, J. Eur. Ceram. Soc. 28 (2008) 871–877.

[2] W. Jo, T. Granzow, E. Aulbach, J. Rödel, D. Damjanovic, Origin of the large strain response in $(K_{0.5}Na_{0.5})NbO_3$-modified $(Bi_{0.5}Na_{0.5})TiO_3$-$BaTiO_3$ lead-free piezoceramics, J. Appl. Phys. 105 (2009) 094102.

[3] A. Ullah, C.W. Ahn, A. Ullah, I.W. Kim, Large strain under a low electric field in lead-free bismuth-based piezoelectrics, Appl. Phys. Lett. 103 (2013) 022906.

[4] J. Fu, R.Z. Zuo, Giant electrostrains accompanying the evolution of a relaxor behavior in Bi(Mg,Ti)O_3-$PbZrO_3$-$PbTiO_3$ ferroelectric ceramics, Acta Mater. 61 (2013) 3687–3694.

[5] J.G. Hao, B. Shen, J.W. Zhai, H.D. Chen, Phase transitional behavior and electric field-induced large strain in alkali niobate-modified $Bi_{0.5}(Na_{0.80}K_{0.20})_{0.5}TiO_3$ lead-free piezoceramics, J. Appl. Phys. 115 (2014) 034101.

[6] W.L. Zhao, R.Z. Zuo, J. Fu, M. Shi, Large strains accompanying field-induced ergodic phase-polar ordered phase transformations in $Bi(Mg_{0.5}Ti_{0.5})O_3$-$PbTiO_3$-$(Bi_{0.5}Na_{0.5})TiO_3$ ternary system, J. Eur. Ceram. Soc. 34 (2014) 2299–2309.

[7] G.Z. Dong, H.Q. Fan, J. Shi, M.M. Li, Composition- and temperature-dependent large strain in $(1-x)(0.8Bi_{0.5}Na_{0.5}TiO_3$-$0.2Bi_{0.5}K_{0.5}TiO_3)$-$xNaNbO_3$ ceramics, J. Eur. Ceram. Soc. 98 (2015) 1150–1155.

[8] H. Simon, J.E. Daniels, J. Glaum, A.J. Studer, J.L. Jones, M. Hoffman, Origin of large recoverable strain in $0.94(Bi_{0.5}Na_{0.5})TiO_3$-$0.06BaTiO_3$ near the ferroelectric-relaxor transition, Appl. Phys. Lett. 102 (2013) 062902.

[9] A. Ullah, R.A. Malik, A. Ullah, D.S. Lee, S.J. Jeong, J.S. Lee, I.W. Kim, C.W. Ahn, Electric-field-induced phase transition and large strain in lead-free Nb-doped BNKT-BST ceramics, J. Eur. Ceram. Soc. 34 (2014) 29–35.

[10] W.L. Zhao, R.Z. Zuo, J. Fu, Temperature-insensitive large electrostrains and electric field induced intermediate phases in $(0.7-x)Bi(Mg_{1/2}Ti_{1/2})TiO_3$-$xPb(Mg_{1/3}Nb_{2/3})O_3$-$0.3PbTiO_3$ ceramics, J. Eur. Ceram. Soc. 34 (2014) 4235–4245.

[11] W.F. Bai, Y.L. Bian, J.H. Hao, B. Shen, J.W. Zhai, The composition and temperature-dependent structure evolution and large strain response in $(1-x)(Bi_{0.5}Na_{0.5})TiO_3$-$xBa(Al_{0.5}Ta_{0.5})O_3$ ceramics, J. Eur. Ceram. Soc. 96 (2013) 246–252.

[12] K.S. Hong, S.E. Park, Phase relations in the system of $(Na_{1/2}Bi_{1/2})TiO_3$-$PbTiO_3$II. Dielectric property, J. Appl. Phys. 79 (1996) 388–392.

[13] S.W. Choi, T.R. Shrout, S.J. Jang, A.S. Bhalla, Dielectric and pyroelectric properties in the $Pb(Mg_{1/3}Nb_{2/3})O_3$-$PbTiO_3$ system, Ferroelectrics 100 (1989) 29–38.

[14] X.M. Liu, H.Z. Guo, X.L. Tan, Evolution of structure and electrical properties with lanthanum content in $[(Bi_{1/2}Na_{1/2})_{0.95}Ba_{0.05}]_{1-x}La_xTiO_3$ ceramics, J. Eur. Ceram. Soc. 34 (2014) 2997–3006.

[15] A. Singh, R. Chatterjee, 0.40% bipolar strain in lead-free BNT-KNN system modified with Li, Ta and Sb, J. Am. Ceram. Soc. 96 (2013) 509–512.

[16] W.L. Zhao, R.Z. Zuo, D.G. Zheng, L.T. Li, Dielectric relaxor evolution and frequency-insensitive giant strains in $(Bi_{0.5}Na_{0.5})TiO_3$-modified $Bi(Mg_{0.5}Ti_{0.5})O_3$-$PbTiO_3$ ferroelectric ceramics, J. Eur. Ceram. Soc. 97 (2014) 1855–1860.

[17] D. Viehland, S.J. Jang, L.E. Cross, M. Wuttig, Freezing of the polarization fluctuations in lead magnesium niobate relaxors, J. Appl. Phys. 68 (1990) 2916–2921.

[18] X.H. Dai, A. DiGiovanni, D. Viehland, Dielectric properties of tetragonal lanthanum modified lead zirconate titanate ceramics, J. Appl. Phys 74 (1993) 3399–3405.

[19] A.A. Bokov, Z.G. Ye, Recent progress in relaxor ferroelectrics with perovskite structure, J. Mater. Sci. 41 (2006) 31–52.
[20] G. Burns, F.H. Dacol, Crystalline ferroelectrics with glassy polarization behavior, Phys. Rev. B 28 (1983) 2527–2530.
[21] C. Ang, Z. Jing, Z. Yu, Ferroelectric relaxor Ba(Ti,Ce)O_3, J. Phys.: Condens. Matter. 14 (2002) 8901–8912.
[22] V. Westphal, W. Kleemann, Diffuse phase transition and random-field-induced domain state, Phys. Rev. Lett. 68 (1992) 847–850.
[23] S. Tinte, B.P. Burton, E. Cockayne, U.V. Waghmare, Origin of the relaxor state in Pb($B_xB'_{1-x}$)O_3 perovskites, Phys. Rev. Lett. 97 (2006) 137601.
[24] D.S. Fu, H. Taniguchi, M. Itoh, S.Y. Koshihara, N. Yamamoto, S. Mori, Relaxor Pb($Mg_{1/3}Nb_{2/3}$)O_3: a ferroelectric with multiple inhomogeneities, Phys. Rev. Lett. 103 (2009) 207601.
[25] S. Schaab, T. Granzow, Temperature dependent switching mechanism of ($Pb_{0.92}La_{0.08}$)$Zr_{0.65}Ti_{0.35}$)O_3 investigated by small and large signal measurements, Appl. Phys. Lett. 97 (2010) 132902.
[26] E. Sapper, N. Novak, W. Jo, T. Granzow, J. Rödel, Electric-field-temperature phase diagram of the ferroelectric relaxor system $(1-x)Bi_{1/2}Na_{1/2}TiO_3$-$x$BaTiO3 doped with manganese, J. Appl. Phys. 115 (2014) 194104.
[27] F. Li, R.Z. Zuo, D.G. Zheng, L.T. Li, Phase-composition-dependent piezoelectric and electromechanical strain properties in ($Bi_{1/2}Na_{1/2}$)TiO_3-Ba($Ni_{1/2}Nb_{1/2}$)O_3 lead-free ceramics, J. Am. Ceram. Soc. 98 (2015) 811–818.
[28] D.G. Zheng, R.Z. Zuo, Relaxor-normal ferroelectric phase transition and significantly enhanced electromechanical strain behavior in Bi($Ni_{1/2}Ti_{1/2}$)O_3-$PbTiO_3$-Pb($Mg_{1/3}Nb_{2/3}$)O_3 ternary system close to the morphotropic phase boundary, J. Eur. Ceram. Soc. 35 (2015) 3485–3493.
[29] S.M. Gupta, J.F. Li, D. Viehland, Coexistence of relaxor and normal ferroelectric phases in morphotropic phase boundary compositions of lanthanum-modified lead zirconate titanate, J. Am. Ceram. Soc. 81 (1998) 557–564.
[30] L.L. Fan, J. Chen, S. Li, H.J. Kang, L.J. Liu, L. Fang, X.R. Xing, Enhanced piezoelectric and ferroelectric properties in the $BaZrO_3$ substituted $BiFeO_3$–$PbTiO_3$, Appl. Phys. Lett. 102 (2013) 022905.
[31] J.E. Daniels, W. Jo, J. Rödel, V. Honkimäki, J.L. Jones, Electric-field-induced phase-change behavior in ($Bi_{0.5}Na_{0.5}$)TiO_3-$BaTiO_3$-($K_{0.5}Na_{0.5}$)NbO_3: a combinatorial investigation, Acta Mater. 58 (2010) 2103–2111.
[32] A. Ullah, A. Ullah, I.W. Kim, D.S. Lee, S.J. Jeong, C.W. Ahn, Large electromechanical response in lead-free la-doped BNKT-BST piezoelectric ceramics, J. Am. Ceram. Soc. 97 (2014) 2471–2478.
[33] M. Roth, E. Mojaev, E. Dul'kin, P. Gemeiner, B. Dkhil, Phase transition at a nanometer scale detected by acoustic emission within the cubic phase Pb($Zn_{1/3}Nb_{2/3}$)O_3-$x$$PbTiO_3$ relaxor ferroelectrics, Phys. Rev. Lett. 98 (2007) 265701.
[34] W. Dmowski, S.B. Vakhrushev, I.K. Jeong, M.P. Hehlen, F. Trouw, T. Egami, Local lattice dynamics and the origin of the relaxor ferroelectric behavior, Phys. Rev. Lett. 100 (2008) 137602.
[35] S. Teanishi, M. Suzuki, Y. Noguchi, M. Miyayama, C. Moriyoshi, Y. Kuroiwa, K. Tawa, S. Mori, Giant strain in lead-free ($Bi_{0.5}Na_{0.5}$)TiO_3-based single crystals, Appl. Phys. Lett. 92 (2008) 182905.
[36] D. Maurya, Y. Zhou, Y.J. Wang, Y.K. Yan, J.F. Li, D. Viehland, S. Priya, Giant strain with ultra-low hysteresis and high temperature stability in grain oriented lead-free $K_{0.5}Bi_{0.5}TiO_3$-$BaTiO_3$-$Na_{0.5}Bi_{0.5}TiO_3$ piezoelectric materials, Sci. Rep. 5 (2015) 8595.